

Expedited thermalization dynamics in incommensurate systems

Mingdi Xu,¹ Zijun Wei,¹ Xiang-Ping Jiang,^{2,*} and Lei Pan^{1,†}

¹*School of Physics, Nankai University, Tianjin 300071, China*

²*School of Physics, Hangzhou Normal University, Hangzhou, Zhejiang 311121, China*

We study the thermalization dynamics of a quantum system embedded in an incommensurate potential and coupled to a Markovian thermal reservoir. The dephasing induced by the bath drives the system toward an infinite-temperature steady state, erasing all initial information-including signatures of localization. We find that initially localized states can relax to the homogeneous steady state faster than delocalized states. Moreover, low-temperature initial states thermalize to infinite temperature more rapidly than high-temperature states—a phenomenon reminiscent of the Mpemba effect, where hotter liquids freeze faster than warmer ones. The slowest relaxation mode in the Liouvillian plays critical role in the expedited thermalization for localized or cold initial states. Our results reveal that the combination of disordered structure and environmental dissipation may lead to non-trivial thermalization behavior, which advances both the conceptual framework of the Mpemba effect and the theoretical understanding of nonequilibrium processes in dissipative disordered systems.

I. INTRODUCTION

Nonequilibrium physics, and particularly nonequilibrium dynamics, constitutes a long-standing yet perpetually vibrant research frontier that spans nearly all branches of physics. In contrast to equilibrium systems, nonequilibrium dynamics inherently involves all degrees of freedom, precluding a complete thermodynamic description via partition-function-based methods in statistics mechanics. This intrinsic complexity positions nonequilibrium dynamics among the most fundamental challenges in modern physics. Recent advances in quantum gas microscopy and controlling parameters of the system have enabled unprecedented experimental access to non-equilibrium dynamics in diverse quantum systems. Nonequilibrium dynamics have uncovered a host of exotic physical effects such as quantum many-body scarring [1–4], and Kardar-Parisi-Zhang universality [5–8].

A non-intuitive relaxation phenomenon in nonequilibrium dynamics is the Mpemba effect wherein initially warmer liquids undergo faster cooling to a target temperature than their cooler counterparts under identical external conditions. Experimental observations of the Mpemba effect span classical systems [10–19]. Conversely, an inverse Mpemba effect where a colder system heats up faster than a warmer one has been theoretically predicted [20, 21] and recently confirmed experimentally [22]. Recently, the discovery of quantum version of Mpemba effects has been achieved through both theoretical proposals and experimental realizations [23–25] in well-controlled quantum systems. The experimental realization of quantum Mpemba effects has stimulated substantial theoretical investigations into their underlying mechanisms [26], spanning integrable systems [27–30], many-body localizations [31], random circuits

[32, 33] and diverse physical platforms [34–42]. Conversely, an inverse Mpemba effect where a colder system heats up faster than a warmer one has been theoretically predicted [20, 21] and recently confirmed experimentally [22]. A natural theoretical framework for describing quantum Mpemba effects (QME) or inverse QME is through open quantum systems. Quantum dissipative dynamics for open quantum systems plays a pivotal role in nonequilibrium statistical physics, offering a window into emergent phenomena such as thermalization and information scrambling. This approach provides a powerful paradigm to characterize the QME through comparing thermalization pathways from initial states at different temperatures and investigating the role of decoherence in relaxation processes. Since the impact of thermal bath, a quantum system with initial information such as localization properties should become delocalized completely throughout the entire system. This occurs because local dephasing mechanisms inevitably drive quantum systems toward infinite-temperature states, regardless of their Hamiltonian structure.

Localization serves as a fundamental mechanism that breaks quantum thermalization, profoundly affecting both charge transport and thermalization dynamics in quantum systems. Previous research on many-body localized systems coupled to external reservoirs has demonstrated that environmental interactions destroy localization, ultimately leading to thermal equilibrium. However, localized systems display characteristic slower relaxation, which fundamentally differs from the thermalization dynamics observed in ergodic system. Hence, general expectations suggest that extended states (closer to the steady state in configuration space) or high-temperature states should relax faster. Motivated by recent advances in open disordered quantum systems [43–66] and the experimental realization of quantum Mpemba effects [23–25], we investigate the thermalization dynamics in open quantum systems with incommensurate potentials, aiming to identify potential Mpemba-like behavior. Specifically, we investigate which reaches the maxi-

* 2015iopjxp@gmail.com

† panlei@nankai.edu.cn

mally mixed state faster than the initial localized state or the extended state and whether the low-temperature or high-temperature initial state is heated to infinite temperature more rapidly.

II. THEORETICAL FRAMEWORK AND MODEL

A natural framework for describing the inverse Mpemba effect lies in investigating the dissipative dynamics of open quantum systems. Consider a quantum system interacting with an environment, where the total Hamiltonian H_T takes the form

$$H_T = H_S + H_E + H_{SE}, \quad (1)$$

with H_S and H_E denoting the system and environment Hamiltonians, respectively, while H_{SE} accounts for their interaction. Under the Born-Markov approximation [67, 68], tracing out the environmental degrees of freedom leads to a Lindblad master equation [69, 70] describing the system's time evolution

$$\frac{d\rho(t)}{dt} = \mathcal{L}[\rho(t)] = -i[H_S, \rho(t)] + \mathcal{D}[\rho(t)], \quad (2)$$

where $\rho(t)$ is the system's density matrix, and \mathcal{L} denotes the Liouvillian superoperator which is a mathematical mapping that transforms one matrix into another with trace and positive-definition conserving. The first term governs unitary dynamics, whereas $\mathcal{D}[\rho(t)]$ encodes dissipative effects

$$\mathcal{D}[\rho(t)] = \sum_j \sum_{m=1}^M \Gamma_j^{(m)} \left(O_j^{(m)} \rho O_j^{(m)\dagger} - \frac{1}{2} \{ O_j^{(m)\dagger} O_j^{(m)}, \rho \} \right). \quad (3)$$

Here $\{A, B\} \equiv AB + BA$ is the anticommutator, $O_j^{(m)}$ are called dissipation operator or quantum jump operator, j labels lattice sites, and M indicates the number of dissipation channels per site with dissipation strength $\Gamma_j^{(m)}$. The open quantum system's evolution is dictated by the spectrum of superoperator \mathcal{L} , with the formal solution $\rho(t)e = e^{\mathcal{L}t}[\rho_0]$. At long times, the system approaches a steady state $\rho_{ss} = \lim_{t \rightarrow \infty} \rho(t)$, corresponding to the zero-eigenvalue eigenvector of \mathcal{L} . The nature of this steady state is influenced by the specific jump operators in \mathcal{L} . The dynamics governed by the master equation admits a spectral decomposition solution

$$\rho(t) = \rho_{ss} + \sum_{n=2}^{d^2} \text{Tr}(l_n \rho_0) r_n e^{\lambda_n t}, \quad (4)$$

where d denotes the Hilbert space dimension, ρ_0 the initial density operator, while r_n and l_n represent respectively the right and left eigenvectors of the Liouvillian superoperator \mathcal{L} with eigenvalues λ_k , satisfying $\mathcal{L}[r_n] = \lambda_n r_n$ and $\mathcal{L}^\dagger[l_n] = \lambda_n l_n$. These eigenvalues are ordered by their real components $0 = \lambda_1 < |\text{Re}(\lambda_2)| \leq |\text{Re}(\lambda_3)| \leq \dots \leq |\text{Re}(\lambda_{d^2})|$, all possessing non-positive real parts.

This expansion (4) reveals that the quantum dynamics decomposes into d^2 independent decay channels. The λ_1 channel corresponds to the steady-state solution, while all others exhibit exponential relaxation governed by $e^{\lambda_n t}$. Crucially, the decay rate scales with $|\text{Re}(\lambda_n)|$ meaning larger values indicate faster relaxation. The dominant subleading contribution comes from λ_2 , representing the most persistent non-equilibrium mode.

Next we introduce the system model as will be discussed in this paper. We consider the system subjected to a quasi-periodic potential with system length L which is described by the following Hamiltonian

$$H_S = \sum_j V \cos(\beta j^\alpha) a_j^\dagger a_j + \sum_j^{L-1} t (a_{j+1}^\dagger a_j + a_j^\dagger a_{j+1}). \quad (5)$$

Here, V is the potential strength, t is the hopping amplitude, β and α are real numbers, and j is the site index. When α takes rational values and v is integer-valued, the system reduces to the standard periodic Bloch model. For irrational β with $\alpha \geq 2$ the system produces identical localization behavior to the random Anderson model, exhibiting complete spatial localization with identical localization lengths. The model exhibits a mobility edge within a certain parameter regime ($0 < \alpha < 1, V < 2$ with irrational β) supports mobility edges with the mobility edge at $E_c = \pm(2t - V)$ [71].

We select a specific parameter set that generates a well-defined mobility edge where the potential strength $V = 1.4$, hopping amplitude $t = 1$, quasiperiodic modulation $\beta = 4\pi^2$, $\alpha = 0.7$, and system size $L = 35$. Figure 1(a) displays the calculated inverse participation ratio (IPR), clearly revealing the coexistence of localized and extended states, with the mobility edge separating the two regimes. To further characterize these states, we examine the real-space density matrices of a representative localized state (index $m = 3$) and an extended state (index $m = 16$), which will be utilized in our later analysis. As evident from Fig. 1(a), states near the spectral edges exhibit strong localization, whereas those near the band center remain extended. This distinction is further corroborated by the spatial structure of their density matrices. In Fig. 1(b), the extended state ($m = 16$) displays a broad spatial distribution, with particle density delocalized across multiple lattice sites. In contrast, Fig. 1(c) demonstrates that the localized state ($m = 3$) is confined to a narrow region, with negligible amplitude away from its central site. These observations align with our previous discussion on the energy-dependent localization properties. Remarkably, when studying the dissipative

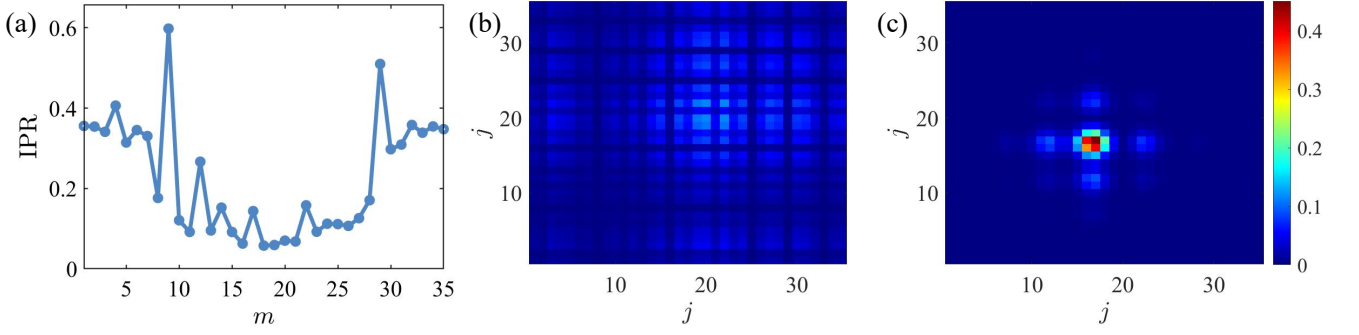


FIG. 1. Mobility Edge Display. (a) The inverse participation ratio (IPR) of the eigenstates of the Hamiltonian, where m denotes the eigenstate index ordered by increasing energy. (b) The site occupation density matrix of the localized state (indexed by $m = 3$), where j denotes the site index. (c) The site occupation density matrix of the extended state (indexed by $m = 16$).

relaxation toward an infinite-temperature steady state, we observe that the localized state—despite initially residing at a lower effective temperature—thermalizes faster than both the high-temperature thermal state and the extended state. This counterintuitive behavior, which we attribute to the inverse QME, highlights the crucial role of localization in dictating nonequilibrium dynamics.

III. EXPEDITED THERMALIZATION AND INVERSE QUANTUM MPEMBA EFFECT

In this section, we investigate heating dynamics induced by quantum dissipation, revealing the inverse QME in such systems. As established previously, the dissipative evolution of the system is governed by the Lindblad master equation (2). For simplicity, we consider the case where each lattice site couples to a single dissipation channel ($M = 1$), with uniform dissipation strength Γ across all sites. We choose the dissipative operator as dephasing, i.e., $O_j = n_j = a_j^\dagger a_j$ for all j . Since the dissipative operator is Hermitian, which ensures that the steady state of the system is the maximally mixed state, also known as the infinite-temperature thermal state (see appendix A). In any basis representation, its steady-state density matrix is

$$\rho_{ss} = \frac{1}{L} \mathbf{I} \quad (6)$$

Here, \mathbf{I} is the identity matrix, whose dimension is equal to the dimension of the system's Hilbert space. Under the influence of above dissipation, the system will be driven to the steady-state ρ_{ss} regardless of its initial state. To quantify the inverse QME, we introduce the Frobenius norm as a measure of the distance between a given state ρ and the steady state ρ_{ss} :

$$\mathcal{D}(\rho) = \|\rho - \rho_{ss}\|_F = \sqrt{\text{Tr}[(\rho - \rho_{ss})^\dagger (\rho - \rho_{ss})]}. \quad (7)$$

The inverse QME manifests when a state initially farther from equilibrium (larger D) relaxes faster than a closer state.

We analyze the time evolution of both the extended (Fig. 1(b)) and localized (Fig. 1(c)) states, comparing their relaxation dynamics with a thermal state at temperature $T_t = 0.25$:

$$\rho_{T_t} = \frac{1}{\mathcal{Z}} \sum_n e^{-E_n/T_t} |n\rangle\langle n|, \quad \mathcal{Z} = \sum_n e^{-E_n/T_t}, \quad (8)$$

where $\{|n\rangle\}$ are Hamiltonian eigenstates with eigenvalues $\{E_n\}$. The thermal state is defined as

$$\rho_{T_t} = \frac{\sum_n e^{-E_n/T_t} |n\rangle\langle n|}{\sum_n e^{-E_n/T_t}} \quad (9)$$

where $\{|n\rangle\}$ are Hamiltonian eigenstates with eigenvalues $\{E_n\}$. T_t is the temperature of the thermal state.

Figure 2 reveals distinct relaxation behaviors for different initial states. The extended state maintains a larger Frobenius distance \mathcal{D} from the steady state compared to the thermal state throughout the entire evolution, both at initial time ($t = 0$) and in the long-time limit ($t \rightarrow \infty$). This persistent separation indicates the absence of inverse QME between these states. More remarkably, while the localized state initially shows greater deviation from equilibrium ($\mathcal{D}_l(0) > \mathcal{D}_t(0)$), its relaxation trajectory crosses that of the thermal state at finite time, ultimately reaching smaller \mathcal{D} values in the long-time regime. This characteristic crossing demonstrates a clear signature of the inverse QME, where the initially more distant localized state thermalizes faster than both the thermal reference state and the extended state. The accelerated relaxation of the localized state occurs despite its greater initial distance from equilibrium, challenging conventional expectations that states farther from equilibrium should take longer to relax.

The temperature analysis further corroborates the existence of the inverse QME in our system. The three initial states exhibit distinct effective temperatures: $T_l = 0.22$ for the localized state, $T_t = 0.25$ for the thermal

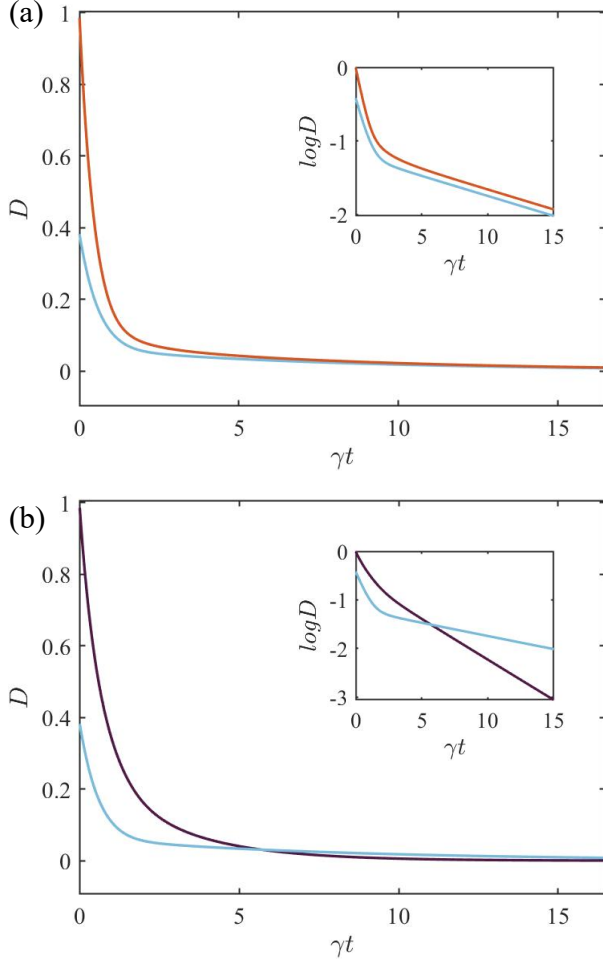


FIG. 2. The temporal evolution of the Frobenius distance. (a) The temporal evolution of the Frobenius distance D between the extended state (indexed by $m = 16, T_e = 9.15$, represented by the orange curve) and the thermal state (at temperature $T_t = 0.25$, represented by the blue curve). The inset in the upper right corner shows the logarithm of the Frobenius distance $\ln D$. It can be clearly seen that the two curves do not intersect, indicating the absence of inverse QME. (b) The temporal evolution of the Frobenius distance between the localized state (indexed by $m = 3, T_l = 0.22$, represented by the red curve) and the thermal state (at temperature $T_t = 0.25$, represented by the blue curve). It can be clearly seen that the two curves intersect, indicating the occurrence of the inverse QME.

state, and $T_e = 9.14$ for the extended state, establishing the clear hierarchy $T_l < T_t < T_e \ll T_{ss} = \infty$. Remarkably, the coldest localized state (T_l) demonstrates the fastest relaxation to the infinite-temperature steady state, violating conventional thermal relaxation expectations. This manifests as two concurrent effects: the localized state thermalizes faster than both the intermediate-temperature thermal state and the much hotter extended state. The persistence of this temperature-inverted relaxation behavior highlights the non-thermal nature of

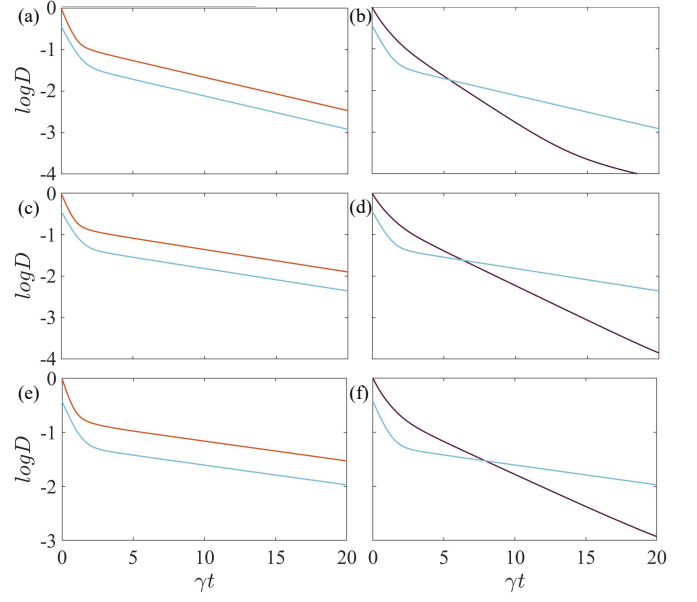


FIG. 3. The temporal evolution of D under different potential strengths V . The orange curves represent the extended states (indexed by $m = 16$), the red curves represent the localized states (indexed by $m = 3$), and the blue curves represent the thermal states (at temperature $T_t = 0.3$). The potential strength V is set to 1.2 in panels (a) and (b), 1.4 in panels (c) and (d), and 1.6 in panels (e) and (f). In all three cases, the localized state temperature is lower than the thermal state temperature, which in turn is lower than the extended state temperature.

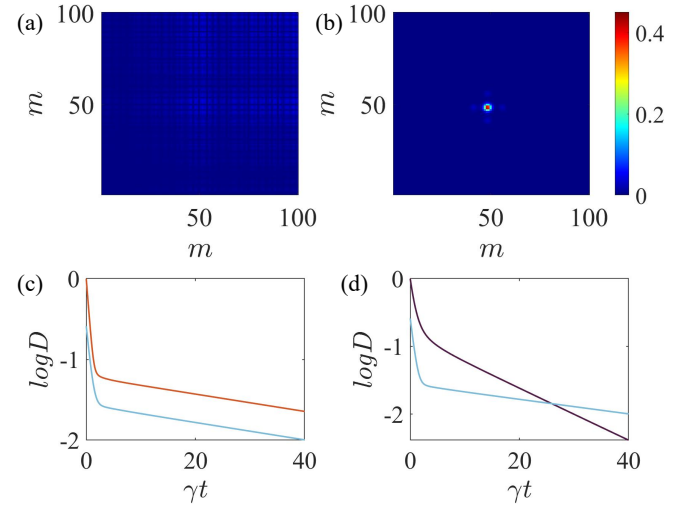


FIG. 4. The inverse QME for a lattice with $L = 100$ sites. (a) is the real-space density matrix of the extended state with energy index $m = 47$, and (b) is the real-space density matrix of the localized state with energy index $m = 7$. (c) shows the temporal evolution of the Frobenius distance between the extended state and the thermal state, and (d) shows the temporal evolution of the Frobenius distance between the localized state and the thermal state. The temperatures of the three initial states are: $T_l = 0.23$, $T_t = 0.3$, $T_e = 12.26$.

inverse QME in our system. The localized state's accelerated dynamics cannot be explained by temperature considerations alone, implying that quantum disordered systems can exhibit fundamentally different thermalization mechanisms that transcend simple temperature-based predictions.

To reveal the physical mechanism of the inverse QME, we revisit the We can find the asymptotic behavior emerges from (4) clearly in the long-time limit

$$\rho(t) \approx \rho_{ss} + e^{\text{Re}(\lambda_2)t} \left[\text{Tr}(l_2 \rho_0) r_2 e^{i\text{Im}(\lambda_2)t} \right], \quad (10)$$

meaning the relaxation speed depends critically on the projection $\text{Tr}(l_2 \rho_0)$ between the initial state and the slowest-decaying mode. Smaller overlap values lead to faster equilibration, as the system requires less time to relax to the steady-state. This is crucial for understanding the mechanisms behind accelerated thermalization and the inverse QME. Our analysis demonstrates that localized initial states exhibit markedly weaker overlap with r_2 compared to their extended counterparts, explaining their accelerated approach to steady-state despite appearing more distant in certain physical metrics.

It is worth to emphasis that the inverse QME demonstrated in our system exhibits remarkable robustness against parameter variations. As shown in Fig. 3, the characteristic relaxation behavior persists across a finite range of potential strengths V , with the localized state consistently showing accelerated thermalization compared to both thermal and extended states. This parametric stability suggests that the observed phenomenon is not fine-tuned but rather a generic feature of the system's dissipative dynamics.

Furthermore, the effect maintains its distinctive signature in larger systems. Numerical simulations for a lattice of $L = 100$ sites (Fig. 4) confirm that the essential physics remains unchanged: the localized state at lower effective temperature ($T_l = 0.22$) continues to thermalize faster than higher-temperature states. This system-size independence demonstrates that the QME is not merely a finite-size artifact but persists in the thermodynamic limit, reinforcing its significance as a genuine non-equilibrium quantum phenomenon.

The combination of parameter robustness and scalability with system size provides strong evidence that the observed inverse QME represents a fundamental characteristic of dissipative quantum systems with localized states, rather than a special case limited to specific parameters or small systems.

IV. CONCLUSION AND OUTLOOK

In this work, we have systematically investigated the thermalization dynamics of quantum systems embedded in incommensurate potentials and coupled to Markovian reservoirs, uncovering a robust inverse QME where initially colder and more localized states thermalize faster

to infinite temperature than their warmer and extended counterparts. Through a combination of analytical and numerical approaches, we have demonstrated that this counterintuitive behavior stems from the reduced overlap between localized states and the slowest-decaying Liouvillian modes, providing a clear physical mechanism for the accelerated thermalization. The effect persists across parameter variations and system sizes, indicating its fundamental nature in dissipative quantum systems with localization properties.

Our findings advance the understanding of nonequilibrium dynamics and establish a connection between quantum localization and anomalous thermalization phenomena. They demonstrate that temperature hierarchy alone cannot predict relaxation timescales in quantum systems.

Our work can be directly extend to other localized systems with different disorder potentials which can be experimentally realized in cold atom systems using existing techniques for engineering disorder or quasiperiodic potentials and controlled dissipation [72–82].

The robustness of inverse QME suggests it may be observable in various quantum simulation platforms [83–85], potentially opening new avenues for controlling quantum thermalization processes. Future theoretical work could fruitfully explore the relationship between our findings and other manifestations of the QME across different physical systems, as well as investigate the role of different types of system-environment couplings.

ACKNOWLEDGEMENTS

The work is supported by the National Natural Science Foundation of China (Grant No. 12304290) and the Fundamental Research Funds for the Central Universities.

Appendix A: Proof of maximally mixed steady-state under hermitian dissipation operators

In this appendix, we prove the conclusion that a steady-state is maximally mixed state when dissipation operators are hermitian. For simplicity, we assume the dissipation operator is local dephasing, namely, $O_j = n_j$. Defining the matrix element $\rho_{i,j}(t) = \langle i | \rho(t) | j \rangle$ in the local basis, where $|j\rangle = \hat{c}_j^\dagger |0\rangle$ is the single-particle state at the lattice site j , we can obtain the time evolution equations from the Lindblad master equation

$$\frac{d}{dt} \rho_{i,j} = -iJ(\rho_{i,j+1} + \rho_{i,j-1} - \rho_{i+1,j} - \rho_{i-1,j}) \quad (A1)$$

$$+ i(\epsilon_j - \epsilon_i) \rho_{i,j} - \Gamma \rho_{i,j} (1 - \delta_{i,j}), \quad (A2)$$

where $\delta_{i,j}$ denotes the (Kronecker) delta function. We can prove that the steady-state solution $\hat{\rho}_{ss}$ to above equation which corresponds to $\frac{d}{dt} \rho_{i,j} = 0$ for any ma-

trix element, is the maximally-mixed state, namely the steady-state density matrix ρ_{ss} is proportional to the identity matrix

$$\rho_{ss} = \frac{1}{L} \mathbf{I}. \quad (\text{A3})$$

First, terms $\Gamma \rho_{i,j} (1 - \delta_{i,j})$ in the differential equation (A2) lead to all off-diagonal terms of density matrix $\rho_{i,j}$

($i \neq j$) decay to zero in the steady state, leaving only the diagonal elements. Second, the diagonal elements of steady-state density matrix are uniform due to symmetry. This is because if the diagonal elements are not uniform, the probability distribution on lattice sites would flow from higher-population to lower-population sites due to the symmetric hopping terms in the Hamiltonian, which is in contradiction with the steady-state condition.

-
- [1] H. Bernien, S. Schwartz, A. Keesling, H. Levine, A. Omran, H. Pichler, S. Choi, A. S. Zibrov, M. Endres, M. Greiner, et al., Probing many-body dynamics on a 51-atom quantum simulator, *Nature* **551**, 579 (2017).
 - [2] M. Serbyn, D. A. Abanin, and Z. Papić, Quantum many-body scars and weak breaking of ergodicity, *Nat. Phys.* **17**, 675 (2021).
 - [3] S. Moudgalya, B. A. Bernevig, and N. Regnault, Quantum many-body scars and hilbert space fragmentation: A review of exact results, *Rep. Prog. Phys.* **85**, 086501 (2022).
 - [4] A. Chandran, T. Iadecola, V. Khemani, and R. Moessner, Quantum many-body scars: A quasiparticle perspective, *Annu. Rev. Condens. Matter Phys.* **14**, 443 (2022).
 - [5] M. Ljubotina, M. Žnidarič, and T. Prosen, Kardar-Parisi-Zhang physics in the quantum Heisenberg magnet, *Phys. Rev. Lett.* **122**, 210602 (2019).
 - [6] D. Wei, A. Rubio-Abadal, B. Ye, F. Machado, J. Kemp, K. Srakaew, S. Hollerith, J. Rui, S. Gopalakrishnan, N. Y. Yao, I. Bloch, and J. Zeiher, Quantum gas microscopy of Kardar-Parisi-Zhang superdiffusion, *Science* **376**, 716 (2022).
 - [7] A. Scheie, N. E. Sherman, M. Dupont, S. E. Nagler, M. B. Stone, G. E. Granroth, J. E. Moore, and D. A. Tennant, Detection of Kardar-Parisi-Zhang hydrodynamics in a quantum Heisenberg spin-1/2 chain, *Nat. Phys.* **17**, 726 (2021).
 - [8] Google Quantum AI and Collaborators, Dynamics of magnetization at infinite temperature in a Heisenberg spin chain, *Science* **384**, 48 (2024).
 - [9] E. B. Mpemba and D. G. Osborne, Cool? *Phys. Educ.* **4**, 172 (1969).
 - [10] M. Jeng, The Mpemba effect: When can hot water freeze faster than cold?, *Am. J. Phys.* **74**, 514 (2006).
 - [11] I. Klich, O. Raz, O. Hirschberg, and M. Vucelja, Mpemba index and anomalous relaxation, *Phys. Rev. X* **9**, 021060 (2019).
 - [12] Y.-H. Ahn, H. Kang, D.-Y. Koh, and H. Lee, Experimental verifications of Mpemba-like behaviors of clathrate hydrates, *Korean J. Chem. Eng.* **33**, 1903 (2016).
 - [13] P. Chaddah, S. Dash, K. Kumar, and A. Banerjee, Overtaking while approaching equilibrium, *arXiv:1011.3598*.
 - [14] A. Kumar and J. Bechhoefer, Exponentially faster cooling in a colloidal system, *Nature (London)* **584**, 64 (2020).
 - [15] C. Hu, J. Li, S. Huang, H. Li, C. Luo, J. Chen, S. Jiang, and L. An, Conformation directed Mpemba effect on polylactide crystallization, *Cryst. Growth Des.* **18**, 5757 (2018).
 - [16] J. Liu, J. Li, B. Liu, I. W. Hamley, and S. Jiang, Mpemba effect in crystallization of polybutene-1, *Soft Matter* **19**, 3337 (2023).
 - [17] M. Chorazewski, M. Wasiak, A. V. Sychev, V. I. Korotkovskii, and E. B. Postnikov, The curious case of 1-ethylpyridinium triflate: Ionic liquid exhibiting the Mpemba effect, *J. Solution Chem.* **53**, 80 (2024).
 - [18] Z. Lu and O. Raz, Nonequilibrium thermodynamics of the Markovian Mpemba effect and its inverse, *Proc. Natl. Acad. Sci. U.S.A.* **114**, 5083 (2017).
 - [19] A. Lasanta, F. Vega Reyes, A. Prados, and A. Santos, When the hotter cools more quickly: Mpemba effect in granular fluids, *Phys. Rev. Lett.* **119**, 148001 (2017).
 - [20] Z. Lu and O. Raz, Nonequilibrium thermodynamics of the Markovian Mpemba effect and its inverse, *Proc. Natl. Acad. Sci. U.S.A.* **114**, 5083 (2017).
 - [21] A. Lasanta, F. Vega Reyes, A. Prados, and A. Santos, When the hotter cools more quickly: Mpemba effect in granular fluids, *Phys. Rev. Lett.* **119**, 148001 (2017).
 - [22] A. Kumar, R. Chétrite, and J. Bechhoefer, Anomalous heating in a colloidal system, *Proc. Natl. Acad. Sci. U.S.A.* **119**, e2118484119 (2022).
 - [23] L. Kh. Joshi, J. Franke, A. Rath, F. Ares, S. Murciano, F. Kranzl, R. Blatt, P. Zoller, B. Vermersch, P. Calabrese, C. F. Roos, and M. K. Joshi, Observing the quantum Mpemba effect in quantum simulations, *Phys. Rev. Lett.* **133**, 010402 (2024).
 - [24] S. A. Shapira, Y. Shapira, J. Markov, G. Teza, N. Akerman, O. Raz, and R. Ozeri, The Mpemba effect demonstrated on a single trapped ion qubit, *Phys. Rev. Lett.* **133**, 010403 (2024).
 - [25] J. Zhang, G. Xia, C.-W. Wu, T. Chen, Q. Zhang, Y. Xie, W.-B. Su, W. Wu, C.-W. Qiu, P.-X. Chen, W. Li, H. Jing, and Y.-L. Zhou, Observation of quantum strong Mpemba effect, *Nat. Commun.* **16**, 301 (2025).
 - [26] F. Ares, P. Calabrese, and S. Murciano, The quantum Mpemba effects, *arXiv:2502.08087*
 - [27] S. Murciano, F. Ares, I. Klich, and P. Calabrese, Entanglement asymmetry and quantum Mpemba effect in the XY spin chain, *J. Stat. Mech.* (2024) 013103.
 - [28] K. Chalas, F. Ares, C. Rylands, and P. Calabrese, Multiple crossing during dynamical symmetry restoration and implications for the quantum Mpemba effect, *J. Stat. Mech.* (2024) 103101.
 - [29] C. Rylands, K. Klobas, F. Ares, P. Calabrese, S. Murciano, and B. Bertini, Microscopic origin of the quantum Mpemba effect in integrable systems, *Phys. Rev. Lett.* **133**, 010401 (2024).
 - [30] M. Lastres, S. Murciano, F. Ares, P. Calabrese, Entanglement asymmetry in the critical XXZ spin chain, *J.*

- Stat. Mech.* (2025) 013107.
- [31] S. Liu, H.-K. Zhang, S. Yin, S.-X. Zhang, and H. Yao, Quantum Mpemba effects in many-body localization systems, [arXiv:2408.07750](#).
 - [32] S. Liu, H.-K. Zhang, S. Yin, and S.-X. Zhang, Symmetry restoration and quantum Mpemba effect in symmetric random circuits, *Phys. Rev. Lett.* **133**, 140405 (2024).
 - [33] F. Ares, S. Murciano, P. Calabrese, L. Piroli, Entanglement asymmetry dynamics in random quantum circuits, [arXiv:2501.12459](#)
 - [34] W.-X. Chang, S. Yin, S.-X. Zhang, and Z.-X. Li, Imaginary-time Mpemba effect in quantum many-body system, [arXiv:2409.06547](#).
 - [35] J. W. Dong, H. F. Mu, M. Qin, and H. T. Cui, Quantum Mpemba effect of localization in the dissipative mosaic model, *Phys. Rev. A* **111**, 022215 (2025).
 - [36] M. Fossati, C. Rylands, and P. Calabrese, Entanglement asymmetry in CFT with boundary symmetry breaking, [arXiv:2411.10244](#)
 - [37] S. Longhi, Photonic Mpemba effect, *Opt. Lett.* **49**, 5188 (2024).
 - [38] S. Longhi, Mpemba effect and super-accelerated thermalization in the damped quantum harmonic oscillator, *Quantum* **9**, 1677 (2025).
 - [39] S. Longhi, Quantum Mpemba effect from initial system-reservoir entanglement, [arXiv:2504.21758](#)
 - [40] S. Longhi, Quantum Mpemba effect from initial system-reservoir entanglement, [arXiv:2504.21758](#)
 - [41] X. Wang, J. Su, and J. Wang, Mpemba meets quantum chaos: Anomalous relaxation and Mpemba crossings in dissipative Sachdev-Ye-Kitaev models, [arXiv:2410.06669](#).
 - [42] X. Wang and J. Wang, Mpemba effects in nonequilibrium open quantum systems, *Phys. Rev. Research* **6**, 033330 (2024).
 - [43] R. Hamazaki, K. Kawabata, and M. Ueda, Non-Hermitian Many-Body Localization, *Phys. Rev. Lett.* **123**, 090603 (2019).
 - [44] L.-J. Zhai, S. Yin, and G.-Y. Huang, Many-body localization in a non-Hermitian quasiperiodic system, *Phys. Rev. B* **102**, 064206 (2020).
 - [45] K. Suthar, Y.-C. Wang, Y.-P. Huang, H.-H. Jen, and J.-S. You, Non-Hermitian many-body localization with open boundaries, *Phys. Rev. B* **106**, 0642085 (2022).
 - [46] C. Ehrhardt and J. Larson, Exploring the impact of fluctuation-induced criticality on non-hermitian skin effect and quantum sensors, [arXiv:2310.18259](#) (2023).
 - [47] F. Roccati, F. Balducci, R. Shir, and A. Chenu, Diagnosing non-Hermitian many-body localization and quantum chaos via singular value decomposition, *Phys. Rev. B* **109**, L140201 (2024).
 - [48] D. A. Huse, R. Nandkishore, F. Pietracaprina, V. Ros, and A. Scardicchio, Localized systems coupled to small baths: From Anderson to Zeno, *Phys. Rev. B* **92**, 014203 (2015).
 - [49] A. Purkayastha, A. Dhar, and M. Kulkarni, Nonequilibrium phase diagram of a one-dimensional quasiperiodic system with a single-particle mobility edge, *Phys. Rev. B* **96**, 180204(R) (2017).
 - [50] V. Balachandran, S. R. Clark, J. Goold, and D. Poletti, Energy Current Rectification and Mobility Edges, *Phys. Rev. Lett.* **123**, 020603 (2019).
 - [51] C. Chiaracane, M. T. Mitchison, A. Purkayastha, G. Haack, and J. Goold, Quasiperiodic quantum heat engines with a mobility edge, *Phys. Rev. Research* **2**, 013093 (2020).
 - [52] M. Balasubrahmaniam, S. Mondal, and S. Mujumdar, Necklace-State-Mediated Anomalous Enhancement of Transport in Anderson-Localized non-Hermitian Hybrid Systems, *Phys. Rev. Lett.* **124**, 123901 (2020).
 - [53] S. Weidemann, M. Kremer, S. Longhi, and A. Szameit, Coexistence of dynamical delocalization and spectral localization through stochastic dissipation, *Nat. Photon.* **15**, 576 (2021).
 - [54] A. M. Lacerda, J. Goold, and G. T. Landi, Dephasing enhanced transport in boundary-driven quasiperiodic chains, *Phys. Rev. B* **104**, 174203 (2021).
 - [55] D. Dwiputra and F. P. Zen, Environment-assisted quantum transport and mobility edges, *Phys. Rev. A* **104**, 022205 (2021).
 - [56] M. Saha, B. P. Venkatesh, and B. K. Agarwalla, Quantum transport in quasiperiodic lattice systems in the presence of Büttiker probes, *Phys. Rev. B* **105**, 224204 (2022).
 - [57] C. Chiaracane, A. Purkayastha, M. T. Mitchison, and J. Goold, Dephasing-enhanced performance in quasiperiodic thermal machines, *Phys. Rev. B* **105**, 134203 (2022).
 - [58] S. Longhi, Anderson Localization in Dissipative Lattices, *Ann. Phys.* **535**, 2200658 (2023).
 - [59] S. Longhi, Dephasing-Induced Mobility Edges in Quasicrystals, *Phys. Rev. Lett.* **132**, 236301 (2024).
 - [60] X.-P. Jiang, X. Yang, Y. Hu, L. Pan, Dissipation induced ergodic-nonergodic transitions in finite-height mosaic Wannier-Stark lattices, [arXiv:2407.17301](#) (2024).
 - [61] X. Yang, X.-P. Jiang, Z. Wei, Y. Wang, and L. Pan, Dissipation-induced transition between delocalization and localization in the three-dimensional Anderson model *Phys. Rev. B* **111**, 134203 (2025).
 - [62] C. Wang, and X. R. Wang, Anderson localization transitions in disordered non-Hermitian systems with exceptional points *Phys. Rev. B* **107**, 024202 (2023).
 - [63] L.-J. Zhai, S. Yin, and G.-Y. Huang, Many-body localization in a non-Hermitian quasiperiodic system, *Phys. Rev. B* **102**, 064206 (2020).
 - [64] Y.-C. Wang, K. Suthar, H. H. Jen, Y.-T. Hsu, and J.-S. You, Non-Hermitian skin effects on thermal and many-body localized phases, *Phys. Rev. B* **107**, L220205 (2023).
 - [65] Y. Huang and B. I. Shklovskii, Spectral rigidity of non-Hermitian symmetric random matrices near the Anderson transition, *Phys. Rev. B* **102**, 064212 (2020).
 - [66] Y. Huang and B. I. Shklovskii, Anderson transition in three-dimensional systems with non-Hermitian disorder, *Phys. Rev. B* **101**, 014204 (2020).
 - [67] G. M. Moy, J. J. Hope, and C. M. Savage, Born and Markov approximations for atom lasers, *Phys. Rev. A* **59**, 667 (1999).
 - [68] H.-P. Breuer and F. Petruccione, *The Theory of Open Quantum Systems*, (Oxford University Press, Oxford, 2002).
 - [69] G. Lindblad, On the generators of quantum dynamical semigroups, *Commun. Math. Phys.* **119**, 48 (1976).
 - [70] V. Gorini, A. Kossakowski, and E. C. Sudarsahan, Completely positive dynamical semigroups of N -level systems, *J. Math. Phys.* **17**, 821 (1976).
 - [71] S. D. Sarma, S. He, and X. C. Xie, Mobility edge in a model one-dimensional potential, *Phys. Rev. Lett.* **61**, 2144 (1988).
 - [72] G. Barontini, R. Labouvie, F. Stubenrauch, A. Vogler,

- V. Guarrera, and H. Ott, Controlling the Dynamics of an Open Many-Body Quantum System with Localized Dissipation, *Phys. Rev. Lett.* **110**, 035302 (2013).
- [73] B. Yan, S. A. Moses, B. Gadway, J. P. Covey, K. R. Hazzard, A. M. Rey, D. S. Jin, and J. Ye, Observation of dipolar spin-exchange interactions with lattice-confined polar molecules, *Nature (London)* **501**, 521 (2013).
- [74] Y. S. Patil, S. Chakram, and M. Vengalattore, Measurement-Induced Localization of an Ultracold Lattice Gas, *Phys. Rev. Lett.* **115**, 140402 (2015).
- [75] R. Labouvie, B. Santra, S. Heun, and H. Ott, Bistability in a Driven-Dissipative Superfluid, *Phys. Rev. Lett.* **116**, 235302 (2016).
- [76] T. Tomita, S. Nakajima, I. Danshita, Y. Takasu, and Y. Takahashi, Observation of the Mott insulator to superfluid crossover of a driven-dissipative Bose-Hubbard system, *Sci. Adv.* **3**, e1701513 (2017).
- [77] H. P. Lüschen, P. Bordia, S. S. Hodgman, M. Schreiber, S. Sarkar, A. J. Daley, M. H. Fischer, E. Altman, I. Bloch, and U. Schneider, Signatures of Many-Body Localization in a Controlled Open Quantum System, *Phys. Rev. X* **7**, 011034 (2017).
- [78] K. Sponselee, L. Freystatzky, B. Abeln, M. Diem, B. Hundt, A. Kochanke, T. Ponath, B. Santra, L. Mathey, K. Sengstock, and C. Becker, Dynamics of ultracold quantum gases in the dissipative Fermi-Hubbard model, *Quantum Sci. Technol.* **4**, 014002 (2018).
- [79] T. Tomita, S. Nakajima, Y. Takasu, and Y. Takahashi, Dissipative Bose-Hubbard system with intrinsic two-body loss, *Phys. Rev. A* **99**, 031601(R) (2019).
- [80] Y. Takasu, T. Yagami, Y. Ashida, R. Hamazaki, Y. Kuno, and Y. Takahashi, PT-symmetric non-Hermitian quantum many-body system using ultracold atoms in an optical lattice with controlled dissipation, *Prog. Theor. Exp. Phys.* **2020**, 12A110 (2020).
- [81] R. Bouganne, M. B. Aguilera, A. Ghermaoui, and F. Gerbier, Anomalous decay of coherence in a dissipative many-body system, *Nat. Phys.* **16**, 21 (2020).
- [82] Y. Zhao, Y. Tian, J. Ye, Y. Wu, Z. Zhao, Z. Chi, T. Tian, H. Yao, J. Hu, Y. Chen, and W. Chen, Observation of universal dissipative dynamics in strongly correlated quantum gas, *arXiv:2309.10257* (2023).
- [83] F. Schäfer, T. Fukuhara, S. Sugawa, Y. Takasu, and Y. Takahashi, Tools for quantum simulation with ultracold atoms in optical lattices, *Nat. Rev. Phys.* **2**, 411 (2020).
- [84] M. Müller, S. Diehl, G. Pupillo, and P. Zoller, Engineered Open Systems and Quantum Simulations with Atoms and Ions, *Adv. At. Mol. Opt. Phys.* **61**, 1-80 (2012).
- [85] P. M. Harrington, E. J. Mueller, and K. W. Murch, Engineered dissipation for quantum information science, *Nat. Rev. Phys.* **4**, 660 (2022).